Oxygen vacancies effects on phase diagram of epitaxial $La_{1-x}Sr_xMnO_3$ thin films

Wan Qian, Jin KuiJuan, Li QingQing, Feng YaQing, Wang Can, Ge Chen, He Meng, Lu HuiBin, Guo HaiZhong, Li XiaoLong, Yang YuPing and Yang GuoZhen

Citation: SCIENCE CHINA Physics, Mechanics & Astronomy **60**, 057711 (2017); doi: 10.1007/s11433-017-9018-8

View online: http://engine.scichina.com/doi/10.1007/s11433-017-9018-8

View Table of Contents:http://engine.scichina.com/publisher/scp/journal/SCPMA/60/5

Published by the Science China Press

SCIENCE CHINA
Physics, Mechanics & Astronomy

SCIENCE CHINA
Physics, Mechanics & Astronomy

• Article •

May 2017 Vol. 60 No. 5: 057711
doi: 10.1007/s11433-017-9018-8

Oxygen vacancies effects on phase diagram of epitaxial $La_{1-x}Sr_xMnO_3$ thin films

Qian Wan[1,2], KuiJuan Jin[1,2,3*], QingQing Li[1,4], YaQing Feng[1,2], Can Wang[1,2], Chen Ge[1], Meng He[1], HuiBin Lu[1], HaiZhong Guo[1*], XiaoLong Li[5], YuPing Yang[4], and GuoZhen Yang[1,2,3]

[1] *Institute of Physics, Chinese Academy of Sciences, Beijing 100190, China;*
[2] *University of Chinese Academy of Sciences, Beijing 100049, China;*
[3] *Collaborative Innovation Center of Quantum Matter, Beijing 100190, China;*
[4] *School of Science, Minzu University of China, Beijing 100081, China;*
[5] *Shanghai Synchrotron Radiation Facility (SSRF), Shanghai Institute of Applied Physics, Chinese Academy of Sciences, Shanghai 201204, China*

Received January 13, 2017; accepted March 3, 2017; published online March 22, 2017

We investigated the effects of oxygen vacancies on the structural, magnetic, and transport properties of $La_{1-x}Sr_xMnO_3$ (x=0.1, 0.2, 0.33, 0.4, and 0.5) grown around a critical point (without/with oxygen vacancies) under low oxygen pressure (10 Pa) and high oxygen pressure (40 Pa). We found that all films exhibit ferromagnetic behavior below the magnetic critical temperature, and that the films grown under low oxygen pressures have degraded magnetic properties with lower Curie temperatures and smaller magnetic moments. These results show that in epitaxial $La_{1-x}Sr_xMnO_3$ thin films, the magnetic and transport properties are very sensitive to doping concentration and oxygen vacancies. Phase diagrams of the films based on the doping concentration and oxygen vacancies were plotted and discussed.

$La_{1-x}Sr_xMnO_3$, thin films, phase diagram, oxygen vacancies

PACS number(s): 72.80.Ga, 75.47.Lx, 73.43.Qt, 74.62.Dh

Citation: Q. Wan, K. J. Jin, Q. Q. Li, Y. Q. Feng, C. Wang, C. Ge, M. He, H. B. Lu, H. Z. Guo, X. L. Li, Y. P. Yang, and G. Z. Yang, Oxygen vacancies effects on phase diagram of epitaxial $La_{1-x}Sr_xMnO_3$ thin films, Sci. China-Phys. Mech. Astron. **60**, 057711 (2017), doi: 10.1007/s11433-017-9018-8

1 Introduction

Hole-doped perovskite manganese oxides, $Re_{1-x}A_xMnO_3$ (where *Re*=rare earth and *A*=alkaline earth), exhibit a fantastically rich variety of intrinsically related structural, magnetic, and transport properties. These can be controlled in various ways: doping x, temperature, magnetic field, electric field, and photo excitation [1-9]. This variety arises from delicate interactions among electronic, magnetic, orbital, and structural degrees of freedom to deliver exotic, coexisting magnetic and electronic phases. Desirable tunable properties, such as colossal magnetoresistance and half-metallicity of $La_{1-x}Sr_xMnO_3$ (LSMO, a prototype of the family of $Re_{1-x}A_xMnO_3$) are promising for multifunctional devices [10-12]. The parent compound $LaMnO_3$ is an antiferromagnetic insulator, but $La_{1-x}Sr_xMnO_3$ exhibits fascinating phase diagrams that include a well-known ferromagnetic phase that spans a robust range of electronic densities [2,13,14]. For many potential technological applications, such as magnetoresistive sensors and magnetic random-access memory,

*Corresponding authors (KuiJuan Jin, email: kjjin@iphy.ac.cn; HaiZhong Guo, email: hguo@iphy.ac.cn)

high-quality thin films and heterostructures are highly desirable. In particular, thin films and heterostructures provide the possibility of externally modifying their properties by epitaxial strain, and thus potentially generating novel properties at the interfaces, opening a new perspective for a variety of important experimental investigations [15-17].

In epitaxial manganite thin films, the epitaxial strain can be induced by the film growth parameters, including lattice mismatch, film thickness, oxygen content, and doping concentration. The phase diagram of LSMO shows that its electrical and magnetic properties are strongly dependent on the Mn nominal valence, which in turn is strongly correlated with the doping concentration [2,13,14].

Additionally, oxygen vacancies, which are introduced in perovskite oxide thin films and heterostructures during deposition, play a crucial role in regulating the properties of oxide films and heterostructures [18]. Two main aspects govern the effects of oxygen vacancies on the properties of oxide films and heterostructures. On the one hand, oxygen vacancies can regulate the properties of oxide films and heterostructures to bring out novel phenomena, properties, and various possibilities for multifunctional device applications [19-22]. On the other hand, oxygen vacancies induce degraded ferromagnetism and transport properties in perovskite manganite films and heterostructures [23-25]. It was reported that oxygen vacancies and cation off-stoichiometry would be induced in LSMO films with oxygen pressure below 26 Pa, resulting in the degraded ferromagnetism and insulating states [26].

To address the effects of oxygen vacancies and doping concentration on material properties, $La_{1-x}Sr_xMnO_3$ films with different Sr doping concentrations (x=0.1, 0.2, 0.33, 0.4, and 0.5) were grown under low oxygen pressure (10 Pa, LP) and high oxygen pressure (40 Pa, HP). We also fixed the other film growth parameters of lattice mismatch, film thickness, and substrate temperature to obtain further insight on the effects of the doping concentration and oxygen vacancies on the lattice structure, magnetic, and transport properties of epitaxial LSMO thin films.

2 Experimental details

Epitaxial $La_{1-x}Sr_xMnO_3$ (x=0.1, 0.2, 0.33, 0.4, and 0.5) thin films were grown on (001) $SrTiO_3$ (STO) single crystal substrates by a laser molecular-beam epitaxial system (Laser-MBE, Pascal) combined with a high-pressure reflected high-energy electron diffraction (RHEED) and a laser diode substrate-heating unit at 800°C using an excimer XeCl laser (1.5 J/cm^2, 308 nm, 2 Hz). The two-dimensional layer-by-layer growth mode was monitored by RHEED oscillation. The crystalline quality and out-of-plane lattice constant of the LSMO thin films were identified by high-resolution synchrotron X-ray diffractometry (SXRD) at the BL14B1 beam line of the Shanghai Synchrotron Radiation Facility (SSRF), using a 1.24 Å X-rays with a Huber 5021 six-axes diffractometry. The magnetic and transport properties measurements were performed with a commercial physical properties measurement system (PPMS, Quantum Design Inc.).

3 Results and discussion

The SXRD θ-2θ scan curves of the $La_{1-x}Sr_xMnO_3$ thin films grown under oxygen pressures of 10 Pa (red) and 40 Pa (blue) with different Sr dopings are shown in Figures 1(a)-(e). Only (00l) reflections from the films and the substrates are ob-served. No diffraction peaks from secondary phase or randomly oriented grains are observed, indicating that all the LSMO thin films were epitaxially grown along the c-axis orientation with a good single phase. The doping-dependent c-axis lattice constants deduced from the SXRD patterns are shown in Figure 1(f) where it can be seen that the c-axis lattice constants decrease with increasing Sr doping concentration. It is also obvious in the inset of Figure 1 that the (002) reflection angle of the LSMO films grown under 10 Pa is smaller than that grown under 40 Pa. This result indicates that the out-of-plane lattice constants of the LSMO films with same Sr doping concentration grown under lower pressures are larger than those grown under higher oxygen pressures. Since oxygen vacancies exist in the LSMO films grown with oxygen pressure below 26 Pa [26], we would ascribe this expansion of the lattice constants of the LSMO grown under 10 Pa to the effect of oxygen vacancies.

To investigate the effects of Sr concentration and oxygen vacancies on magnetic properties of LSMO thin films, we measured the temperature dependence of the magnetization of the $La_{1-x}Sr_xMnO_3$ thin films grown under LP and HP with different Sr doping concentrations. The temperature dependence of macroscopic magnetization $M(T)$ were measured with an applied magnetic field of 100 Oe (zero-field cooling (ZFC) and field cooling (FC)), as shown in Figures 2(a)-(e). Comparing the LSMO films grown under LP and HP with the same doping concentrations, it can be seen that the HP LSMO films display the typical $M(T)$ curves and sharp paramagnetic-to-ferromagnetic phase transitions. Whereas, $M(T)$ curves of the LP LSMO films differ from typical ferromagnetic behavior by exhibiting degraded magnetic properties such as a broad paramagnetic-to-ferromagnetic crossover with relatively small magnetization values.

We also plotted the doping dependence of T_C, paramagnetic-to-ferromagnetic phase transition temperature (Figure 2(f)). Here, T_C is defined as the temperature at which (dM/dT) reaches the extreme value. It can be clearly seen from Figure 2(f) that T_C reaches maximum around x=0.33 in the HP LSMO films, and the T_C of the HP LSMO films is lar-

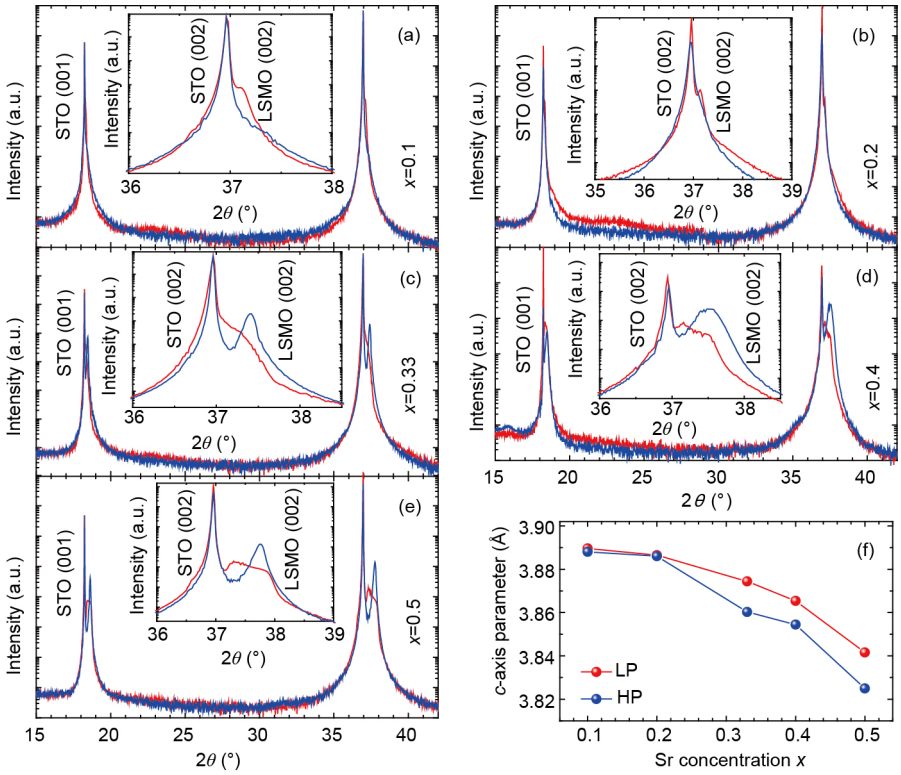

Figure 1 (Color online) SXRD θ-2θ scan curves of the $La_{1-x}Sr_xMnO_3$ thin films grown under oxygen pressures of 10 Pa (red) and 40 Pa (blue) with different Sr doping concentrations: (a) x=0.1; (b) x=0.2; (c) x=0.33; (d) x=0.4; (e) x=0.5. (f) The doping-dependent c-axis lattice constants deduced from the SXRD patterns.

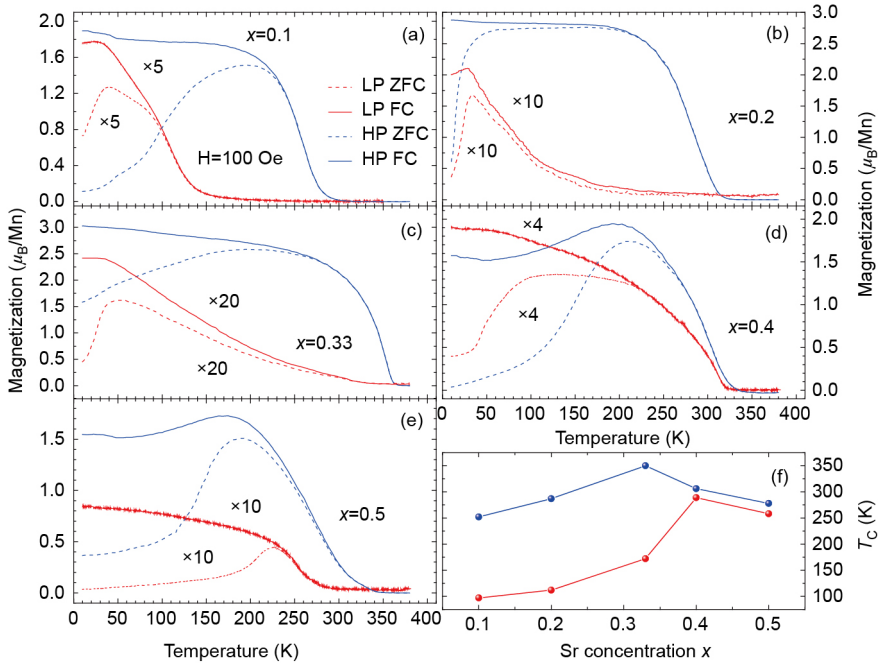

Figure 2 (Color online) Magnetizations versus temperature with an applied magnetic field of 100 Oe (zero-field cooling (ZFC) and field cooling (FC)) for the $La_{1-x}Sr_xMnO_3$ thin films with different Sr dopings: (a) x=0.1; (b) x=0.2; (c) x=0.33; (d) x=0.4; (e) x=0.5. (f) The doping-dependent magnetization deduced from magnetizations versus temperature.

ger than that of the LP LSMO films with same doping concentration. It is well known that the ferromagnetic double exchange (DE) reaches maximum around x=1/3 (x=0.33) and that T_C does so around x=1/3 [27]. Even so, all the LP and HP LSMO films are ferromagnetic below T_C (i.e., they exhibit ferromagnetic hysteresis loops at low temperature). The hys-

teresis loops at 10 K are shown in Figures 3(a) (LP LSMO films) and (b) (HP LSMO films). The relationships of the Sr concentration and the coercive field (H_C), and the saturation magnetizations (M_S) deduced from Figures 3(a) and (b) are respectively displayed in Figures 3(c) and (d). Compared to the HP LSMO films, the hysteresis loops of the LP LSMO films are degraded and sheared with larger coercive fields and smaller saturation magnetizations. For example, H_C is about 95 Oe and M_S is about 3.54μ_B/Mn for the HP LSMO film for which x=0.33, which approaches the bulk value (11/3μ_B/Mn) [2]. However, H_C is about 465 Oe and M_S is about 0.66μ_B/Mn for the LP LSMO film for which x=0.33.

The magneto transport properties as functions of temperature and magnetic field were measured by a standard four-point probe method using PPMS. The temperature dependence of the resistivity of the LSMO films at 0, 3, and 5 T are presented in Figure 4. Here it can be seen that the resistivity found for the LP LSMO films are higher than for the

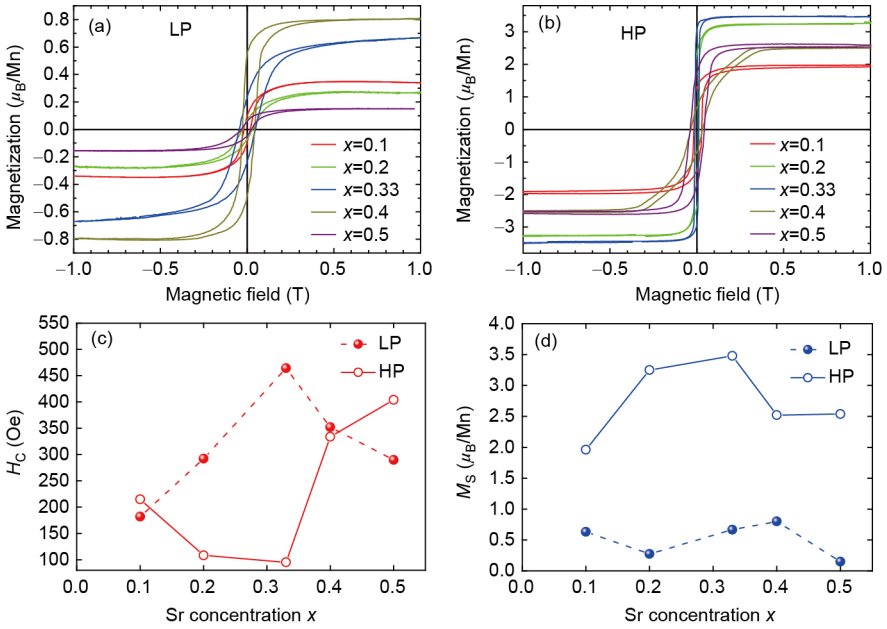

Figure 3 (Color online) The magnetic hysteresis loops $M(H)$ measured between –1 and 1 T fields at 10 K for different Sr concentrations of the $La_{1-x}Sr_xMnO_3$ thin films grown under LP (a) and HP (b); (c) the doping-dependent coercive fields (H_C) deduced from the magnetic hysteresis loops; (d) the doping-dependent saturation magnetizations (M_S) deduced from the magnetic hysteresis loops.

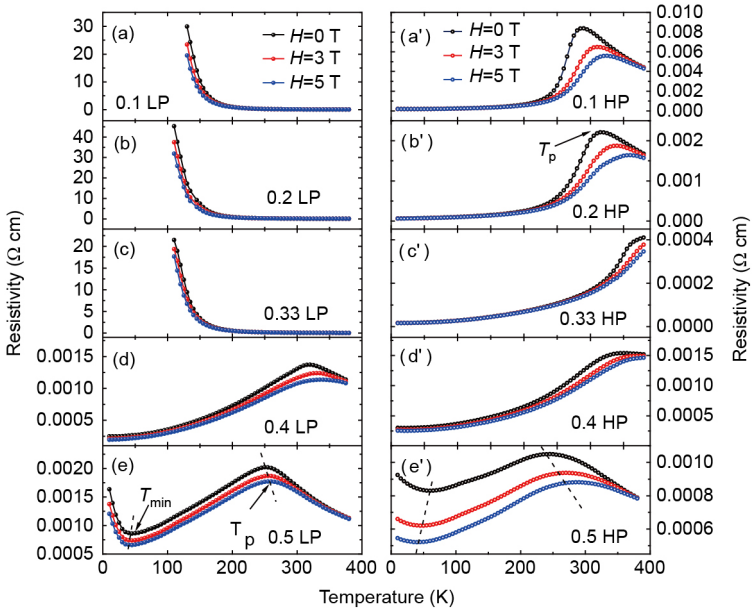

Figure 4 (Color online) Temperature dependence of the resistance of LSMO thin films with different Sr doping concentrations under LP (a)-(e) and HP (a′)-(e′), respectively. The resistance was measured at 0 (black), 3 (red), and 5 T (blue), respectively.

HP ones with the same Sr concentration at same temperature, from five orders of magnitude when x=0.1-0.33 to almost same order of magnitude when x=0.4 and x=0.5. The three LP LSMO films for which x=0.1-0.33 exhibit insulating behavior, whereas the HP LSMO films for which x=0.1 and x=0.2 show a transition from high-temperature insulator to metal, accompanied by the paramagnetic-to-ferromagnetic occurring around T_C, and the HP LSMO film for which x=0.33 displays a metallic behavior throughout the entire measured regime. Both the LP and HP films for which x=0.4 exhibit a transition from high-temperature insulator to metal with resistivity at almost the same order of magnitude, although the temperature of the metal-to-insulator transition (T_P) in the HP LSMO film is slightly higher than in the LP one.

However, at half doping (x=0.5), both the LP and HP LSMO films exhibit complex transport behavior. The temperature-dependent resistivity of the LP and HP LSMO films for which x=0.5 can be divided into three distinct regimes: insulator at high-temperature regime transferring into metal (T_P); at intermediate-temperature regime accompanied by the paramagnetic-to-ferromagnetic transfer occurring around T_C; and the transferrence to an insulator at low-temperature regime while exhibiting a well-defined resistivity minimum at T_{min}. The T_P and T_{min} determined from the transport measurements at H=0 T are 41 and 252 K for the $La_{0.5}Sr_{0.5}MnO_3$ grown under LP, and 60 and 242 K for the $La_{0.5}Sr_{0.5}MnO_3$ grown under HP. One can also see from Figure 4 that T_P increases with the increasing applied magnetic field whereas T_{min} decreases with the increasing applied magnetic field.

These complex transport behaviors in $La_{0.5}Sr_{0.5}MnO_3$ films have also been observed in other manganite thin films [28-30]. Vaz et al. [28] attributed the phase transition around T_{min} to resonant phonon coupling between the substrate and the LSMO film, because the T_{min} of the LSMO/STO film is close to the cubic-to-tetragonal transition of the STO substrate. However, they couldn't explain the same transport phenomena observed in the LSMO/LSAT substrates. Phase separation in manganites at heavy doping level is believed to be one of the mechanisms that induce this complex transport behavior [31].

The resistivity of the LSMO films decreases by applied magnetic fields, which is well known as colossal magnetoresistance (CMR). The temperature dependence of magnetoresistance (MR) of LSMO thin films with different doping Sr concentrations are shown in Figure 5, where the MR ratio is defined as $100\%\times[R(0)–R(H)]/R(H)$. It can be seen from Figure 5 that the magnitude of the magnetoresistance varies across the films. The peak positions of the MR are close to T_C and T_P, and they shift toward higher temperatures in the HP films than the LP films with fixed doping levels. These results well coincide with those of the $M(T)$ data, which suggests that the double exchange mechanism and oxygen vacancies play crucial roles in manganite thin films.

Thus far, we have described the relationships between doping levels and oxygen vacancies and the magnetic and transport properties. Now we discuss how these two important factors directly affect these properties. In our previous work, we discussed oxygen effects on electronic and magnetic properties [32]. The oxygen vacancies induce a weakening of the Mn-O-Mn hybridized bond and an increase in the concentration of Mn^{3+} ions; they also impair the double exchange between Mn^{3+} and Mn^{4+}. In these ways they lead to the transition from metal to insulator and the degraded magnetic properties in the $La_{2/3}Sr_{1/3}MnO_3$ films. The parent compound $LaMnO_3$

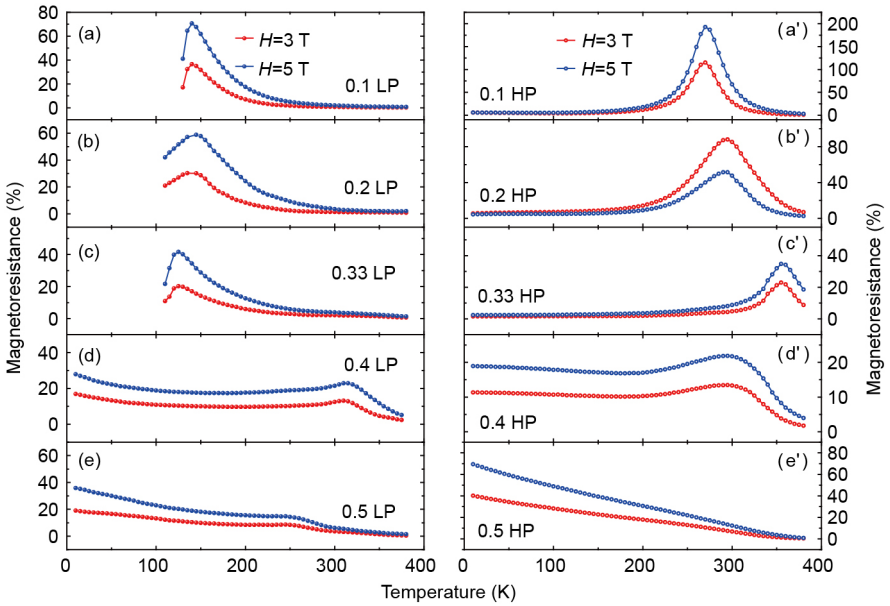

Figure 5 (Color online) Temperature dependence of the magnetoresistance of LSMO thin films with different Sr doping concentrations under LP (a)-(e) and HP (a′)-(e′). The magnetoresistance ratio is defined as $100\%\times[R(0)–R(H)]/R(H)$.

is known as a charge-transfer insulator and antiferromagnet. The gap is between the oxygen p-like state and the unoccupied d-like upper Hubbard band. Sr doping induces holes in the oxygen sites. As Sr doping increases, more holes appear in the oxygen sites; the gap decreases and finally disappears; and then the $La_{1-x}Sr_xMnO_3$ system transfers from insulator to metal. And at the same time, Sr doping induces the some Mn^{3+} ions transfer to Mn^{4+} ions and establishes an Mn^{3+}-O^{2-}-Mn^{4+} exchange interaction. At this point, the $La_{1-x}Sr_xMnO_3$ system becomes ferromagnetism.

4 Summary

In this paper, we investigated the effects of doping level and oxygen vacancies on the magnetic and transport properties of $La_{1-x}Sr_xMnO_3$ films (x=0.1, 0.2, 0.33, 0.4, and 0.5) grown under low oxygen pressure and high oxygen pressure. The structural, transport, and magnetic properties were tuned by the doping concentration and oxygen vacancies, which indicated that the double exchange mechanism and oxygen vacancies play crucial roles in manganite thin films. A phase diagram of the manganese films based on the doping concentrations and oxygen vacancies was established.

This work was supported by the National Key Basic Research Program of China (Grant Nos. 2014CB921001, and 2013CB328706), the Key Research Program of Frontier Sciences of the Chinese Academy of Sciences (Grant No. QYZDJ-SSW-SLH020), the Strategic Priority Research Program (B) of the Chinese Academy of Sciences (Grant No. XDB07030200), and the National Natural Science Foundation of China (Grant Nos. 11574365, 11474349, 11674385, and 11404380). The authors would like to thank the BL14B1 beam line of the Shanghai Synchrotron Radiation Facility and the beam lines of the Beijing Synchrotron Radiation Facility for technical support.

1 P. Mandal, and S. Das, Phys. Rev. B **56**, 15073 (1997).
2 A. Urushibara, Y. Moritomo, T. Arima, A. Asamitsu, G. Kido, and Y. Tokura, Phys. Rev. B **51**, 14103 (1995).
3 T. T. Shang, X. Y. Liu, and L. Gu, Sci. China-Phys. Mech. Astron. **59**, 697001 (2016).
4 X. X. Chen, G. Z. Liu, X. Zhu, J. Qiu, J. L. Yao, M. Zhao, Y. C. Jiang, R. Zhao, and J. Gao, Sci. China-Phys. Mech. Astron. **59**, 677521 (2016).
5 T. Elovaara, H. Huhtinen, S. Majumdar, and P. Paturi, J. Phys.-Condens. Matter **24**, 216002 (2012).
6 A. Asamitsu, Y. Tomioka, H. Kuwahara, and Y. Tokura, Nature **388**, 50 (1997).
7 B. B. Van Aken, T. T. M. Palstra, A. Filippetti, and N. A. Spaldin, Nat. Mater. **3**, 164 (2004).
8 X. Z. Tian, L. F. Wang, X. M. Li, J. K. Wei, S. Z. Yang, Z. Xu, W. L. Wang, and X. D. Bai, Sci. China-Phys. Mech. Astron. **56**, 2361 (2013).
9 K. Miyano, T. Tanaka, Y. Tomioka, and Y. Tokura, Phys. Rev. Lett. **78**, 4257 (1997).
10 J. H. Park, E. Vescovo, H. J. Kim, C. Kwon, R. Ramesh, and T. Venkatesan, Nature **392**, 794 (1998).
11 C. Israel, M. J. Calderón, and N. D. Mathur, Mater. Today **10**, 24 (2007).
12 A. M. Haghiri-Gosnet, and J. P. Renard, J. Phys. D-Appl. Phys. **36**, R127 (2003).
13 A. Asamitsu, Y. Moritomo, R. Kumai, Y. Tomioka, and Y. Tokura, Phys. Rev. B **54**, 1716 (1996).
14 J. Hemberger, A. Krimmel, T. Kurz, H. A. Krug Von Nidda, V. Y. Ivanov, A. A. Mukhin, A. M. Balbashov, and A. Loidl, Phys. Rev. B **66**, 094410 (2002).
15 A. Ohtomo, and H. Y. Hwang, Nature **441**, 120 (2006).
16 H. Yamada, M. Kawasaki, T. Lottermoser, T. Arima, and Y. Tokura, Appl. Phys. Lett. **89**, 052506 (2006).
17 A. Bhattacharya, S. J. May, S. G. E. Te Velthuis, M. Warusawithana, X. Zhai, B. Jiang, J. M. Zuo, M. R. Fitzsimmons, S. D. Bader, and J. N. Eckstein, Phys. Rev. Lett. **100**, 257203 (2008), arXiv: 0710.1452.
18 J. N. Eckstein, Nat. Mater. **6**, 473 (2007).
19 D. A. Muller, N. Nakagawa, A. Ohtomo, J. L. Grazul, and H. Y. Hwang, Nature **430**, 657 (2004).
20 F. Yang, K. J. Jin, H. B. Lu, M. He, C. Wang, J. Wen, and G. Z. Yang, Sci. China-Phys. Mech. Astron. **53**, 852 (2010).
21 Z. Xu, K. Jin, L. Gu, Y. Jin, C. Ge, C. Wang, H. Guo, H. Lu, R. Zhao, and G. Yang, Small **8**, 1279 (2012).
22 P. Gao, Z. Kang, W. Fu, W. Wang, X. Bai, and E. Wang, J. Am. Chem. Soc. **132**, 4197 (2010).
23 M. Rajeswari, R. Shreekala, A. Goyal, S. E. Lofland, S. M. Bhagat, K. Ghosh, R. P. Sharma, R. L. Greene, R. Ramesh, T. Venkatesan, and T. Boettcher, Appl. Phys. Lett. **73**, 2672 (1998).
24 S. Picozzi, C. Ma, Z. Yang, R. Bertacco, M. Cantoni, A. Cattoni, D. Petti, S. Brivio, and F. Ciccacci, Phys. Rev. B **75**, 094418 (2007).
25 R. Zhao, K. Jin, Z. Xu, H. Guo, L. Wang, C. Ge, H. Lu, and G. Yang, Appl. Phys. Lett. **102**, 122402 (2013).
26 Z. Li, M. Bosman, Z. Yang, P. Ren, L. Wang, L. Cao, X. Yu, C. Ke, M. B. H. Breese, A. Rusydi, W. Zhu, Z. Dong, and Y. L. Foo, Adv. Funct. Mater. **22**, 4312 (2012).
27 R. Maezono, S. Ishihara, and N. Nagaosa, Phys. Rev. B **58**, 11583 (1998).
28 C. A. F. Vaz, J. A. Moyer, D. A. Arena, C. H. Ahn, and V. E. Henrich, Phys. Rev. B **90**, 024414 (2014).
29 X. Yin, M. A. Majidi, X. Chi, P. Ren, L. You, N. Palina, X. Yu, C. Diao, D. Schmidt, B. Wang, P. Yang, M. B. H. Breese, J. Wang, and A. Rusydi, NPG Asia Mater. **7**, e196 (2015).
30 V. Markovich, G. Jung, Y. Yuzhelevskii, G. Gorodetsky, F. X. Hu, and J. Gao, Phys. Rev. B **75**, 104419 (2007).
31 E. Dagotto, *Nanoscale phase separation and colossal magnetoresistance* (Springer, New York, 2003).
32 H. Guo, J. Wang, X. He, Z. Yang, Q. Zhang, K. Jin, C. Ge, R. Zhao, L. Gu, Y. Feng, W. Zhou, X. Li, Q. Wan, M. He, C. Hong, Z. Guo, C. Wang, H. Lu, K. Ibrahim, S. Meng, H. Yang, and G. Yang, Adv. Mater. Interfaces **3**, 1500753 (2016).